

# Realistic Actor-Critic: A Framework for Balance Between Value Overestimation and Underestimation

Sicen Li<sup>1</sup> · Qinyun Tang<sup>1</sup> · Yiming Pang<sup>1</sup> · Xinmeng Ma<sup>1</sup> · and Gang Wang<sup>\*2</sup>

Received: date / Accepted: date

**Abstract** This paper proposes a reinforcement learning framework to enhance the exploration-exploitation trade-off by learning a range of policies concerning various confidence bounds. The underestimated values provide stable updates but suffer from inefficient exploration behaviors. On the other hand, overestimated values can help the agent escape local optima, but it might cause over-exploration on low-value areas and function approximation errors accumulation. Algorithms have been proposed to mitigate the above contradiction. However, we lack an understanding of how the value bias impact performance and a method for efficient exploration while keeping value away from catastrophic overestimation bias accumulation. In this paper, we 1) highlight that both under- and overestimation bias can improve learning efficiency, and it is a particular form of the exploration-exploitation dilemma; 2) propose a unified framework called Realistic Actor-Critic(RAC), which employs Universal Value Function Approximators (UVFA) to simultaneously learn policies with different value confidence-bond with the same neural net-

An early preprint is available on arXiv(<https://arxiv.org/abs/2110.09712>) with CC BY: Creative Commons Attribution License. This work has been submitted to the Springer Nature for possible publication. Copyright may be transferred without notice, after which this version may no longer be accessible. This work was supported in part by the National Natural Science Foundation of China under Grant 51779059, in part by the National Natural Science Foundation of Heilongjiang Province (Grant No.YQ2020E028), and National Key Research and Development Project (Grant No.2018YFF01012900). All correspondences should be sent to G. Wang with email: wanggang@hrbeu.edu.cn

<sup>1</sup>College of Mechanical and Electrical Engineering, Harbin Engineering University, Harbin 150001, China: {ihuhuhu, 993740540, pangyiming, mxm2012071615}@hrbeu.edu.cn ·

<sup>2</sup>College of Shipbuilding Engineering, Harbin Engineering University, Harbin 150001, China: wanggang@hrbeu.edu.cn

work, each with a different under-overestimation trade-off. This allows us to perform directed exploration without over-exploration using the upper bounds while still avoiding overestimation using the lower bounds. Through carefully designed experiments, We empirically verify that RAC achieves 10x sample efficiency and 25% performance improvement compared to Soft Actor-Critic on the most challenging Humanoid environment. All the source codes are available at <https://github.com/ihuhuhu/RAC>.

**Keywords** Reinforcement learning(RL) · estimation bias · exploration-exploitation dilemma · realistic actor-critic(RAC)

## 1 Introduction

Sample efficiency is one of the main challenges that prevent reinforcement learning(RL) from applying to real-world systems where obtaining samples is expensive [1, 2, 3]. This paper aims at mitigating this problem by a better balance between exploration and exploitation.

Undesirable overestimation bias and accumulation of function approximation errors in temporal difference methods may lead to sub-optimal policy updates and divergent behaviors [4, 5, 6]. Most model-free off-policy RL methods learn approximate lower confidence bound of Q-function [7, 6, 8, 9, 10] to avoid overestimation by introducing underestimation bias.

However, if the lower bound has a spurious maximum, it will discourage policy to explore potential higher uncertain regions, resulting in stochastic local-maximum and causing pessimistic underexploration [11]. Moreover, directionally uninformed [11] policies, such as Gaus-

sian policies, are unable to avoid fully explored actions, which are wasteful.

Optimistic exploration methods [12, 13, 14] learn upper confidence bounds of the Q-function from an epistemic uncertainty estimate. These methods are directionally informed and encourage policy to execute overestimated actions to help agents escape local optimum. However, such upper confidence bound might cause an agent to over-explore low-value regions. In addition, it increases the risk of value overestimation since transitions with high uncertainty may have higher function approximation errors to make the value overestimated.

To avoid the above problems, one has to adjust hyperparameters carefully and control the bias to keep the value at a balance point between lower and higher bounds: supporting stable learning while providing good exploration behaviors. We highlight that this balance is a particular form of the exploration-exploitation dilemma [3]. Unfortunately, most prior works have studied the overestimation and pessimistic underexploration in isolation and have ignored the under-overestimation trade-off aspect.

We formulate Realistic Actor-Critic (RAC), whose main idea is to learn together values and policies with different trade-offs between underestimation and overestimation in the same network. Policies guided by lower bounds control overestimation bias to provide consistency and stable convergence. Each policy guided by different upper bounds provides a unique exploration strategy to generate overestimated actions, so that the policy family can directionally explore overestimated state-action pairs uniformly and avoid over-exploration. All transitions are stored in a shared replay buffer, and all policies benefit from them to escape spurious maximum.

Such a family of policies is jointly parameterized with the Universal Value Function Approximators (UVFA) [15]. The learning process can be considered as a set of auxiliary tasks [16, 17] that help build shared state representations and sills.

However, learning such policies with diverse behaviors in a single network is challenging since policies vary widely in behavior. We introduce punished Bellman backup, which calculate uncertainty as punishment to correct value estimations. Punished Bellman backup provide fine-granular estimation control to make value approximation shift smoothly between upper and lower bounds, allowing for more efficient training. An ensemble of critics is learned to produce well-calibrated uncertainty estimations (i.e., standard deviation) on unseen samples [8, 13, 18]. We show empirically that RAC controls the std and the mean of value estimate bias to

close to zero for most of the training. Benefit from well bias control, critics are trained with a high Update-To-Data (UTD) ratio [9] to improve sample efficiency significantly.

Empirically, we implement RAC with SAC [19] and TD3 [6] in continuous control benchmarks (OpenAI Gym [20], MuJoCo [21]). Results demonstrate that RAC significantly improves the performance and sample efficiency of SAC and TD3. RAC outperforms the current state-of-the-art algorithms (MBPO [22], REDQ [9] and TQC [10]), achieving state-of-the-art sample efficiency on the Humanoid benchmark. We perform ablations and isolate the effect of the main components of RAC on performance. Moreover, we perform hyperparameter ablations and demonstrate that RAC is stable in practice.

This paper makes the following **contributions**:

- (i) using a conditional architecture with shared weights to learn a family of policies with respect to various confidence bounds that maintain uniformly exploration and stable updates;
- (ii) defining a variant of soft Bellman backup to provide fine granular bias control to smooth value approximations that can make the learning process more efficiently; and
- (iii) experimental evidence that the performance and sample efficiency of the proposed method are better than state-of-the-art methods on continuous control tasks.

The paper is organized as follows. Section 2 describes related works and their results. Section 3 describes the problem setting and preliminaries of RL. Section 4 explains the under-overestimation trade-off. Section 5 introduces the punished Bellman backup and RAC algorithm. Section 6 presents experimental results that show the sample efficacy and final performance of RAC. Finally, Section 7 presents our conclusions.

## 2 Related works

### Underestimation and overestimation of Q-function.

The maximization update rule in Q-learning has been shown to suffer from overestimation bias which will seriously hinder learning [4].

Minimizing the value ensemble is a standard method to deal with overestimation bias. Clipped double Q-learning (CDQ) [6] takes the minimum value between a pair of critics to limit overestimation. SAC [19] then combined CDQ with entropy maximization to get impressive performance in continuous control tasks. Maxmin Q-learning [7] mitigated the overestimation bias by using a minimization over multiple action-value estimates.

But minimizing a Q-function set is unable to filter out abnormally small values, which causes undesired pessimistic underexploration problem [11]. Using minimization to control overestimation is coarse and wasteful as it ignores all estimates except the minimal one [10].

REDQ [9] proposed in-target minimization, which used a minimization across a random subset of Q functions from the ensemble to alleviate the above problems. REDQ [9] showed their method reduces the std of the Q-function bias to close to zero for most of the training. Truncated Quantile Critics (TQC) [10] truncates the right tail of the distributional value ensemble by dropping several of the topmost atoms to control overestimation. Weighted bellman backup [8] and uncertainty weighted actor-critic [23] prevents error propagation [24] in Q-learning by reweighing sample transitions based on uncertainty estimations from the ensembles [8] or Monte Carlo dropout [23, 25]. Unlike prior works, our work does not reweight sample transitions but directly adds uncertainty estimations to punish the target value.

The effect of underestimation bias on learning efficiency is environment-dependent [7]. Therefore, it may be hard to choose the suitable parameters to balance under- and overestimation for entirely different environments. Our work proposed to solve this problem by learning about an optimistic and pessimistic policy family

**Ensemble methods.** In deep learning, ensemble methods often used to solve the two key issues, uncertainty estimations [26, 27] and out-of-distribution robustness [28, 29, 30]. In reinforcement learning, using ensemble to enhance value function estimation was widely studied, such as, averaging a Q-ensemble [31, 32], bootstrapped actor-critic architecture [33, 34], calculate uncertainty to reweight sample transitions [8], minimization over ensemble estimates [7, 9] and update the actor with a value ensemble [10, 9].

A high-level policy can be distilled from a policy ensemble [35, 36] by density-based selection [37], selection through elimination [37], choosing action that max all Q-functions [8, 38, 39], Thompson Sampling [38] and sliding-window UCBs [36]. Leveraging uncertainty estimations of the ensemble, [40, 33, 34] simulated training different policies with a multi-head architecture independently to generate diverse exploratory behaviors.

Ensemble methods were also used to learn joint state presentation to improve sample efficiency. There were two main methods: multi-heads [40, 33, 34, 41] and UVFA [15, 16, 36]. This paper uses uncertainty estimation to reduce value overestimation bias, a simple max operator to get the best policy, and learning joint state presentation with UVFA.

**Optimistic exploration.** Pessimistic initialisation [42] and learning policy that maximizes a lower confidence bound value could suffer a pessimistic underexploration problem [11]. Optimistic exploration is a promising solution to ease the above problem by applying the principle of optimism in the face of uncertainty [12]. Disagreement [13] and EMI [14] considered uncertainty as intrinsic motivation to encourage agents to explore the high uncertainty areas of the environment. Uncertainty punishment proposed in this paper can also be a particular intrinsic motivation. Different with [13, 14] which usually choose the weighting  $\geq 0$  to encourage exploration, punished Bellman backup using the weighting  $\leq 0$  to control value bias.

SUNRISE [8] proposed an optimistic exploration that chooses the action that maximizes an upper confidence bound [43] of Q-functions. OAC [11] proposed an off-policy exploration policy that is adjusted to a linear fit of upper bounds to the critic with the maximum Kullback-Leibler(KL) divergence constraining between the exploration policies and the target policy. Most importantly, our work provides a unified framework for the under-overestimation trade-off.

### 3 Problem setting and preliminaries

In this section, we describe the notations and introduce the concept of maximum entropy RL.

#### 3.1 Notation

We consider the standard reinforcement learning notation, with states  $\mathbf{s}$ , actions  $\mathbf{a}$ , reward  $r(\mathbf{s}, \mathbf{a})$ , and dynamics  $p(\mathbf{s}' | \mathbf{s}, \mathbf{a})$ . The discounted return  $R_t = \sum_{k=0}^{\infty} \gamma^k r_k$  is the total accumulated rewards from timestep  $t$ ,  $\gamma \in [0, 1]$  is a discount factor determining the priority of short-term rewards. The objective is to find the optimal policy  $\pi_{\phi}(\mathbf{s} | \mathbf{a})$  with parameters  $\phi$ , which maximizes the expected return  $J(\phi) = \mathbb{E}_{p_{\pi}} [R_t]$ .

#### 3.2 Maximum Entropy RL

The maximum entropy objective [44] encourages the robustness to noise and exploration by maximizing a weighted objective of the reward and the policy entropy:

$$\pi^* = \arg \max_{\pi} \sum_t \mathbb{E}_{\mathbf{s} \sim p, \mathbf{a} \sim \pi} [r(\mathbf{s}, \mathbf{a}) + \alpha \mathcal{H}(\pi(\cdot | \mathbf{s}))], \quad (1)$$

where  $\alpha$  is the temperature parameter used to determine the relative importance of entropy and reward.

Soft Actor-Critic(SAC) [19] seeks to optimize the maximum entropy objective by alternating between a soft policy evaluation and a soft policy improvement. A parameterized soft Q-function  $Q_\theta(\mathbf{s}, \mathbf{a})$ , known as the critic in actor-critic methods, is trained by minimizing the soft Bellman backup:

$$\mathcal{L}_{\text{critic}}(\theta) = \mathbb{E}_{\tau \sim \mathcal{B}}[(Q_\theta(\mathbf{s}, \mathbf{a}) - y)^2], \quad (2)$$

$$y = r - \gamma \mathbb{E}_{\mathbf{a}' \sim \pi_\phi} [Q_{\bar{\theta}}(\mathbf{s}', \mathbf{a}') - \alpha \log \pi_\phi(\mathbf{a}' | \mathbf{s}')], \quad (3)$$

where  $\tau = (\mathbf{s}, \mathbf{a}, r, \mathbf{s}')$  is a transition,  $\mathcal{B}$  is a replay buffer,  $\bar{\theta}$  are the delayed parameters which is updated by exponential moving average  $\bar{\theta} \leftarrow \rho\theta + (1 - \rho)\bar{\theta}$ ,  $\rho$  is the target smoothing coefficient,  $y$  is the target value. The target value  $Q_{\bar{\theta}}(\mathbf{s}', \mathbf{a}')$  is obtained by using two networks  $Q_\theta^1(\mathbf{s}', \mathbf{a}')$  and  $Q_\theta^2(\mathbf{s}', \mathbf{a}')$  with minimum operator:

$$Q_{\bar{\theta}}(\mathbf{s}', \mathbf{a}') = \min(Q_\theta^1(\mathbf{s}', \mathbf{a}'), Q_\theta^2(\mathbf{s}', \mathbf{a}')). \quad (4)$$

The parameterized policy  $\pi_\phi$ , known as the actor, is updated by minimizing the following object:

$$\mathcal{L}_{\text{actor}}(\phi) = \mathbb{E}_{\mathbf{s} \sim \mathcal{B}, \mathbf{a} \sim \pi_\phi} [\alpha \log(\pi_\phi(\mathbf{a} | \mathbf{s})) - Q_\theta(\mathbf{a}, \mathbf{s})]. \quad (5)$$

SAC uses an automate entropy adjusting mechanism to update  $\alpha$  with following objective:

$$\mathcal{L}_{\text{temp}}(\alpha) = \mathbb{E}_{\mathbf{s} \sim \mathcal{B}, \mathbf{a} \sim \pi_\phi} [-\alpha \log \pi_\phi(\mathbf{a} | \mathbf{s}) - \alpha \bar{\mathcal{H}}], \quad (6)$$

where  $\bar{\mathcal{H}}$  is the target entropy.

## 4 Understanding under-overestimation trade-off

This section briefly discusses the estimation bias issue and empirically shows that a better under-overestimation trade-off may improve learning performance.

### 4.1 Under-overestimation trade-off

Under-overestimation trade-off is a special form of the exploration-exploitation dilemma. This is illustrated in Figure 1. At first, the agent starts with a policy  $\pi_{\text{past}}$ , trained with lower bound  $\hat{Q}_{LB}(\mathbf{s}, \mathbf{a})$ , becoming  $\pi_{LB}$ . We divide the current action space into four regions:

- 1) High uncertainty, low-value. Highly stochastic regions also have low values; overestimation bias might cause an agent to over-explore a low-value area.
- 2) High uncertainty, excessive errors. This region has high uncertainty but is full of unseen transitions that can have excessive-high approximation errors, which may cause catastrophic overestimation and need fewer samples.
- 3) High uncertainty, controllable errors. This region has high uncertainty and is closer to the  $\pi_{LB}$ , with controllable approximation errors, needs more samples.
- 4) Full explored. Since  $\pi_{\text{past}}$  is gradually updated to  $\pi_{LB}$ , the area is fully explored and needs less samples.

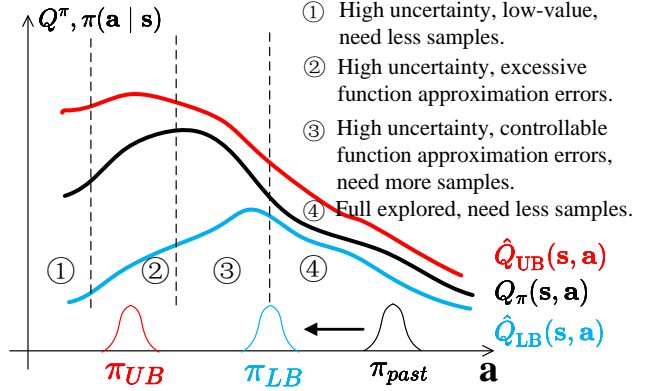


**Fig. 1** The balance between value underestimation and overestimation in actor-critic methods. The state  $s$  is fixed. The graph shows  $Q_\pi$  (in black), which is unknown to the algorithm, estimated lower bound  $\hat{Q}_{LB}$  (in blue), higher bound  $\hat{Q}_{UB}$  (in red), two policies  $\pi_{LB}$  (in blue) and  $\pi_{\text{past}}$  (in black) at different time-steps of the algorithm, exploration policies  $\pi_{UB}$  (in red) for optimistic exploration.

- 3) High uncertainty, controllable errors. This region has high uncertainty and is closer to the  $\pi_{LB}$ , with controllable approximation errors, needs more samples.
- 4) Full explored. Since  $\pi_{\text{past}}$  is gradually updated to  $\pi_{LB}$ , the area is fully explored and needs less samples.

To prevent catastrophic overestimation bias accumulation, SAC [19], TD3 [6] and REDQ [9] introduce underestimation bias to learn lower confidence bounds of Q-functions, similar to equation 4. However, directionally uninformed policies, such as gaussian policies, will sample actions located in region 4 with half probability. If the lower bound has a spurious maximum and policies are directionally uninformed [11], lower bound policy  $\pi_{LB}$  may be stuck at the junction of regions 3 and 4. This is wasteful and inefficient, causing pessimistic underexploration.

$\pi_{UB}$ , which is used in optimistic exploration methods [12, 13, 14], can encourage agents to execute overestimated actions and explore potential high-value regions. But regions with high and overestimated actions, such as region 2, may have excessive function approximation errors. Alternatively, if highly uncertain regions also have low values (like region 1), overestimation bias might cause an agent to over-explore a low-value region.

Ideally, the exploration policies are located in region 3 to provide better exploration behaviors and keep stable updates. There are two ways to achieve this: 1) enforcing a KL constraint between  $\pi_{UB}$  and  $\pi_{LB}$  (like OAC [11]), 2) balancing  $\hat{Q}$  between  $\hat{Q}_{LB}$  and  $\hat{Q}_{UB}$ , and we call it an under-overestimation trade-off.

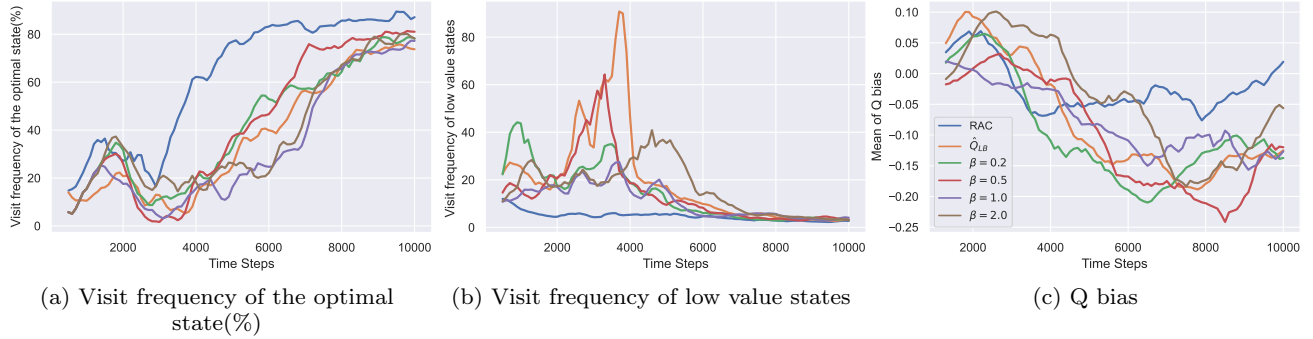


**Fig. 2** Results of the simple MDP. In-target minimization target from REDQ is used as  $\hat{Q}_{LB}$ .  $\hat{Q}_b = \text{mean}(\hat{Q}'_{LB}) + \beta \text{std}(\hat{Q}'_{LB})$  can perform optimistic exploration.  $\beta$  is a key parameter to control value bias. If  $\beta = 0$ ,  $\hat{Q}_b$  is equal to  $\hat{Q}_{LB}$ . As  $\beta$  increases,  $\hat{Q}_b$  gradually approaches  $\hat{Q}_{UB}$ . The horizontal axis indicates the number of time steps. Visit frequency of the optimal state, shown in 2a, is the ratio of the frequency of visiting the optimal state among all termination states. The higher the value, the lower the probability that the agent is stuck in a local optimum. Visit frequency of low value states, shown in 2b, is the ratio of the visit frequency of low value state 2-8 and the optimal state 9. The lower the value, the fewer steps the agent wastes in low-value states. This value has been subtracted by seven, as the minimum step size to reach the optimum state is seven. Q bias, shown in 2c, measures the difference between the estimated Q values and true Q values. All results are estimated by the Monte Carlo method and averaged over eight seeds.

However, in practical applications,  $Q_\pi$  is unknown, and it isn't easy to tune to ideal conditions through constant hyperparameters.

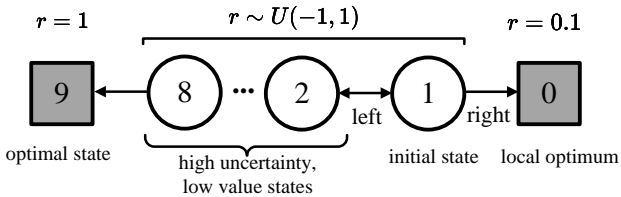


**Fig. 3** A simple episodic MDP [7], adapted from Figure 6.5 in [3]. This MDP has two terminal states: state 9 and state 0. Every episode starts from state 1, which has two actions: Left and Right. The MDP is deterministic. Once the agent takes into any states, the MDP will reward back:  $r = 0.1$  for terminal states 0,  $r = 1$  for terminal states 9 and a reward  $r \sim U(-1, 1)$  for non-terminal states 1-8. State 9 is the optimal state, state 0 is a local optimum, states 1-8 are high uncertainty and low-value states.

## 4.2 A simple MDP

We show this effect in a simple Markov decision process(MDP), shown in Figure 3. Any state's optimal policy is the left action. If the agent wants to go to state 9, it must go through states 1-8 with high uncertainty and low values.

In the experiment, we used a discount factor  $\gamma = 0.9$ ; a replay buffer with size 5000; a boltzmann policy with  $\text{temperature} = 0.1$ ; tabular action-values with

uniform noisy respect to a Uniform distribution  $U(-0.1, 0.1)$ , initialized with a Uniform distribution  $U(-5, 5)$ ; and a learning rate of 0.01 for all algorithms.

The results in Figure 2 verify our hypotheses in Section 4.1. All algorithms converge, but each has a different convergence speed.  $\hat{Q}_{LB}$  underestimates too much and converges to a suboptimal policy in the early learning stage, causing slow convergence. For  $\beta = 0.5$  and 1.0, optimistic exploration drives the agent to escape local optimum and learn faster. However,  $\hat{Q}$  overestimates too much for  $\beta = 2.0$ , significantly impairing the convergence speed of the policy. In addition, no matter what parameter  $\beta$  takes, the agent still over-explore low-value states at different time steps(see figure 2b).

RAC avoids over-exploration in low-value states and is the fastest to converge to the optimal policy. Furthermore, RAC maintains the Q bias close to zero without catastrophic overestimation throughout the learning process, indicating that RAC keeps an outstanding balance between underestimation and overestimation.

## 5 Realistic Actor-Critic

We present Realistic Actor-Critic (RAC), which can be used in conjunction with most modern off-policy actor-critic RL algorithms in principle, such as SAC [19] and TD3 [6]. We describe only the SAC version of RAC (RAC-SAC) in the main body for the exposition. The TD3 version of RAC (RAC-TD3) follows the same principles and is fully described in Appendix B.

### 5.1 Punished Bellman backup

Punished Bellman backup is a variant of soft Bellman backup(2). The idea is to maintain an ensemble of  $N$  soft Q-functions  $Q_{\theta_i}(\mathbf{s}, \mathbf{a})$ , where  $\theta_i$  denote the parameters of the  $i$ -th soft Q-function, which are initialized randomly and independently for inducing an initial diversity in the models [40], but updated with the same target.

Given a transition  $\tau_t$ , punished Bellman backup considers following punished target  $y$ :

$$y = r_t + \gamma \mathbb{E}_{\mathbf{a}' \sim \pi_\phi} [\bar{Q}_{\bar{\theta}}(\mathbf{s}', \mathbf{a}') - \beta \hat{s}(Q_{\bar{\theta}}(\mathbf{s}', \mathbf{a}')) - \alpha \log \pi_\phi(\mathbf{a}' | \mathbf{s}')], \quad (7)$$

where  $\bar{Q}_{\bar{\theta}}(\mathbf{s}, \mathbf{a})$  is the sample mean of the target Q-functions,  $\hat{s}(Q_{\bar{\theta}}(\mathbf{s}, \mathbf{a}))$  is the sample standard deviation of target Q-functions with bessel's correction [45]. Punished Bellman backup uses  $\hat{s}(Q_{\bar{\theta}}(\mathbf{s}, \mathbf{a}))$  as uncertainty estimation to punish value estimation.  $\beta \geq 0$  is the weighting of the punishment. Note that we do not propagate gradient through the uncertainty  $\hat{s}(Q_{\bar{\theta}}(\mathbf{s}, \mathbf{a}))$ .

We write  $Q_{\mathbf{s}\mathbf{a}}^i$  instead of  $Q_{\theta_i}(\mathbf{s}, \mathbf{a})$ ,  $Q_{\mathbf{s}'\mathbf{a}'}^i$  instead of  $Q_{\theta_i}(\mathbf{s}', \mathbf{a}')$  for compactness. Assuming each Q-function has random approximation error  $e_{\mathbf{s}\mathbf{a}}^i$  [4, 7, 9] which is a random variable belonging to some distribution

$$Q_{\mathbf{s}\mathbf{a}}^i = Q_{\mathbf{s}\mathbf{a}}^* + e_{\mathbf{s}\mathbf{a}}^i, \quad (8)$$

where  $Q_{\mathbf{s}\mathbf{a}}^*$  is the ground truth of Q-functions.  $M$  is the number of actions applicable at state  $\mathbf{s}'$ . Define the estimation bias  $Z_{MN}$  for a transition  $\tau_t$  to be

$$\begin{aligned} Z_{MN} &\stackrel{\text{def}}{=} \left[ r + \gamma \max_{\mathbf{a}'} (Q_{\mathbf{s}'\mathbf{a}'}^{mean} - \beta Q_{\mathbf{s}'\mathbf{a}'}^{std}) \right] - \\ &\quad \left( r + \gamma \max_{\mathbf{a}'} Q_{\mathbf{s}'\mathbf{a}'}^* \right) \\ &= \gamma \left[ \max_{\mathbf{a}'} (Q_{\mathbf{s}'\mathbf{a}'}^{mean} - \beta Q_{\mathbf{s}'\mathbf{a}'}^{std}) - \max_{\mathbf{a}'} Q_{\mathbf{s}'\mathbf{a}'}^* \right], \end{aligned} \quad (9)$$

where

$$\begin{aligned} Q_{\mathbf{s}'\mathbf{a}'}^{mean} &\approx \frac{1}{N} \sum_{i=1}^N Q_{\mathbf{s}'\mathbf{a}'}^i = \frac{1}{N} \sum_{i=1}^N (Q_{\mathbf{s}'\mathbf{a}'}^* + e_{\mathbf{s}'\mathbf{a}'}^i) \\ &= Q_{\mathbf{s}'\mathbf{a}'}^* + \frac{1}{N} \sum_{i=1}^N e_{\mathbf{s}'\mathbf{a}'}^i = Q_{\mathbf{s}'\mathbf{a}'}^* + \bar{e}_{\mathbf{s}'\mathbf{a}'}, \end{aligned} \quad (10)$$

### Algorithm 1 RAC: SAC version

---

```

1: Initialize actor network  $\phi$ 
2: Initialize  $N$  critic networks  $\theta_i, i = 1, \dots, N$ 
3: Initialize temperature network  $\psi$ 
4: Initialize empty replay buffer  $\mathcal{B}$ 
5: Initialize target network  $\bar{\theta}_i \leftarrow \theta_i$ , for  $i = 1, 2, \dots, N$ 
6: Initialize uniform distribution  $U_1$  and  $U_2$ 
7: for each iteration do
8:   // OPTIMISTIC EXPLORATION
9:   execute an action  $a \sim \pi_\phi(\cdot | s, \beta)$ ,  $\beta \sim U_2$ .
10:  Observe reward  $r_t$ , new state  $s'$ 
11:  Store transition tuple  $\mathcal{B} \leftarrow \mathcal{B} \cup \{(s, a, r_t, s')\}$ 
12:  for  $G$  updates do
13:    // UPDATE CRITICS VIA PUNISHED BELLMAN
14:    BACKUP
15:    Sample random minibatch:
16:     $\{\tau_j\}_{j=1}^B \sim \mathcal{B}$ ,  $\{\beta_m\}_{m=1}^B \sim U_1$ 
17:    Compute the Q target (15)
18:    for  $i = 1, \dots, N$  do
19:      Update  $\theta_i$  by minimize  $\mathcal{L}_{\text{critic}}^{\text{RAC}}$  (14)
20:    Update target networks:
21:     $\bar{\theta}_i \leftarrow \rho \bar{\theta}_i + (1 - \rho) \theta_i$ 
22:    // UPDATE ACTORS AND TEMPERATURES ACCORDING
23:    TO  $U_1$ 
24:    Update  $\phi$  by minimize  $\mathcal{L}_{\text{actor}}^{\text{RAC-SAC}}$  (16)
25:    Update  $\psi$  by minimize  $\mathcal{L}_{\text{temp}}^{\text{RAC}}$  (13)

```

---

$$\begin{aligned} Q_{\mathbf{s}'\mathbf{a}'}^{std} &\approx \sqrt{\frac{1}{N-1} \sum_{i=1}^N (Q_{\mathbf{s}'\mathbf{a}'}^i - Q_{\mathbf{s}'\mathbf{a}'}^{mean})^2} \\ &= \sqrt{\frac{1}{N-1} \sum_{i=1}^N (Q_{\mathbf{s}'\mathbf{a}'}^* + e_{\mathbf{s}'\mathbf{a}'}^i - Q_{\mathbf{s}'\mathbf{a}'}^* + \bar{e}_{\mathbf{s}'\mathbf{a}'})^2} \\ &= \sqrt{\frac{1}{N-1} \sum_{i=1}^N (e_{\mathbf{s}'\mathbf{a}'}^i - \bar{e}_{\mathbf{s}'\mathbf{a}'})^2} = \hat{s}(e_{\mathbf{s}'\mathbf{a}'}) . \end{aligned} \quad (11)$$

Then

$$Z_{MN} \approx \gamma \left[ \max_{\mathbf{a}'} (Q_{\mathbf{s}'\mathbf{a}'}^* + \bar{e}_{\mathbf{s}'\mathbf{a}'} - \beta \hat{s}(e_{\mathbf{s}'\mathbf{a}'})) - \max_{\mathbf{a}'} Q_{\mathbf{s}'\mathbf{a}'}^* \right]. \quad (12)$$

If one could choose  $\beta = \frac{\bar{e}_{\mathbf{s}'\mathbf{a}'}}{\hat{s}(e_{\mathbf{s}'\mathbf{a}'})}$ ,  $Q_{\mathbf{s}\mathbf{a}}^i$  will be resumed to  $Q_{\mathbf{s}\mathbf{a}}^*$ , then  $Z_{MN}$  can be reduced to near 0. However, it's hard to adjust a suitable constant  $\beta$  for various state-action pairs actually. We develop vanilla RAC which uses a constant  $\beta$  appendix B.3 to research this problem.

**Shifting smoothly between higher and lower bounds.** For  $\beta = 0$ , the update is simple average Q-learning which causes overestimation bias [9]. As  $\beta$  increasing, increasingly penalties  $Q_{\mathbf{s}'\mathbf{a}'}^{std}$  decrease  $E[Z_{MN}]$  gradually, and encourage Q-functions transit smoothly from higher-bounds to lower-bounds.

## 5.2 Realistic Actor-Critic agent

We demonstrate how to use punished Bellman backup to incorporate various bounds of value approximations into a full agent that maintains diverse policies, each with a different under-overestimation trade-off. The pseudocode for RAC-SAC is shown in Algorithm 1.

RAC use UVFA [15] to extend the critic and actor as  $Q_{\theta_i}(\mathbf{s}, \mathbf{a}, \beta)$  and  $\pi_{\phi}(\cdot | \mathbf{s}', \beta)$ ,  $U_1$  is a uniform training distribution  $\mathcal{U}[0, a]$ ,  $a$  is a positive real number,  $\beta \sim U_1$  that generates various bounds of value approximations.

An independent temperature network  $\alpha_{\psi}$  parameterized by  $\psi$  is used to accurately adjust the temperature with respect to  $\beta$ , which can improve the performance of RAC. Then the objective (6) becomes:

$$\mathcal{L}_{\text{temp}}^{\text{RAC}}(\psi) = \mathbb{E}_{\mathbf{s} \sim \mathcal{B}, \mathbf{a} \sim \pi_{\phi}, \beta \sim U_1} [-\alpha_{\psi}(\beta) \log \pi_{\phi}(\mathbf{a} | \mathbf{s}, \beta) - \alpha_{\psi}(\beta) \mathcal{H}]. \quad (13)$$

The extended Q-ensemble use punished Bellman backup to simultaneously approximate a soft Q-function family:

$$\mathcal{L}_{\text{critic}}^{\text{RAC}}(\theta_i) = \mathbb{E}_{\tau \sim \mathcal{B}, \beta \sim U_1} [(Q_{\theta_i}(\mathbf{s}, \mathbf{a}, \beta) - y)^2], \quad (14)$$

$$y = r + \gamma \mathbb{E}_{\mathbf{a}' \sim \pi_{\phi}} [\bar{Q}_{\theta}(\mathbf{s}', \mathbf{a}', \beta) - \beta \hat{s}(Q_{\theta}(\mathbf{s}', \mathbf{a}', \beta)) - \alpha_{\psi}(\beta) \log \pi_{\phi}(\mathbf{a}' | \mathbf{s}', \beta)], \quad (15)$$

where  $\bar{Q}_{\theta}(\mathbf{s}, \mathbf{a}, \beta)$  is the sample mean of target Q-functions,  $\hat{s}(Q_{\theta}(\mathbf{s}, \mathbf{a}, \beta))$  is the corrected sample standard deviation of target Q-functions.

The extended policy  $\pi_{\phi}$  is updated by minimizing the following object:

$$\mathcal{L}_{\text{actor}}^{\text{RAC-SAC}}(\phi) = \mathbb{E}_{\mathbf{s} \sim \mathcal{B}, \beta \sim U_1} [\mathbb{E}_{\mathbf{a} \sim \pi_{\phi}} [\alpha_{\psi}(\beta) \log (\pi_{\phi}(\mathbf{a} | \mathbf{s}, \beta)) - \bar{Q}_{\theta}(\mathbf{a}, \mathbf{s}, \beta)]]], \quad (16)$$

where  $\bar{Q}_{\theta}(\mathbf{a}, \mathbf{s}, \beta)$  is the sample mean of Q-functions.

A larger UTD ratio  $G$  improves sample utilization. We find that a smaller replay buffer capacity slightly improves the sample efficiency of RAC in Section 6.5.

Note that we find that applying different samples, which are generated by binary masks from the Bernoulli distribution [8, 40], to train each Q-function won't improve RAC performance in our experiments; therefore, RAC does not apply this method.

**RAC circumvents direct adjustment of  $\beta$ .** RAC leaners with a distribution of  $\beta$  instead of a constant  $\beta$ . one could evaluate the policy family to find the best  $\beta$ . We employ a discrete number  $H$  of values  $\{\beta_i\}_{i=1}^H$  (see details in Appendix A.1) to implement a distributed evaluation for computational efficiency, and apply the max operator to get best  $\beta$ .

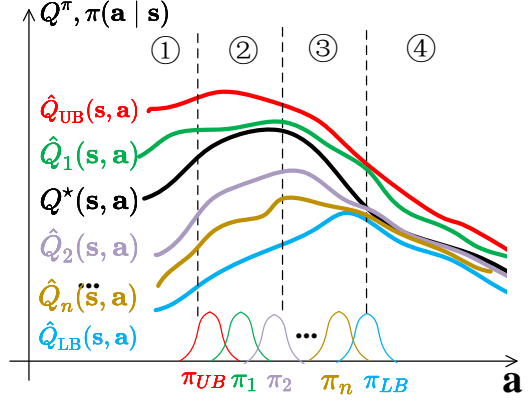


**Fig. 4** Visualization of RAC. The serial numbers in the figure correspond to Section 4.1 and Figure 1. For better illustration,  $\hat{Q}$  is discretized. In fact,  $\hat{Q}_n$  learned by RAC is infinite and changes continuously.  $Q^*(\mathbf{s}, \mathbf{a})$  is the optimal Q-function that is unknown. Q-functions distributed between  $\hat{Q}_{UB}$  and  $\hat{Q}_{LB}$  and their policies distributed between  $\pi_{UB}$  and  $\pi_{LB}$ .  $\pi_{UB}$ ,  $\pi_1$  and  $\pi_2$  are used as exploration policies.

**Optimistic exploration.** When interacting with the environment, we propose to sample  $\beta$  uniformly from a uniform explore distribution  $U_2 = \mathcal{U}[0, b]$ , where  $b < a$  is a positive real number, to get optimistic exploratory behaviors to avoid pessimistic underexploitation [11].

## 5.3 How RAC solves the under-overestimation trade-off

Similar to the idea of NGU [16], RAC decouples exploration and exploitation policies. RAC uses UVFA to simultaneously learn policies with the same neural network, each with different trade-offs between underestimation and overestimation. Using UVFA to learn different degrees of confidence bounds allows us to learn a powerful representation and set of skills that can be quickly transferred to the expected policy. With punished Bellman backup, RAC has a larger number of policies and values that change smoothly, allowing for more efficient training.

This is illustrated in Figure 4. Q-functions that are close to  $\hat{Q}_{LB}$  (like  $\hat{Q}_n$ ) control overestimation bias to provide consistency and stable convergence. Exploration policies (such as  $\pi_{UB}$ ,  $\pi_1$  and  $\pi_2$ ) are far from the spurious maximum of  $\hat{Q}_{LB}$  and  $\hat{Q}_n$ , overestimated actions sampled from them located in regions 1, 2, and 3 lead to a quick correction to the critic estimate. All transitions are stored in a shared replay buffer, and all policies benefit from them to escape spurious maximums. Since exploration policies are not symmetric to the mean of

$\pi_{LB}$  and  $\pi_n$ , RAC also avoids directional uninformedness.

Although RAC cannot always keep the exploration policies located in region 3, the policy family avoids all behaviors concentrated in regions 1 or 2. Exploration behaviors uniformly distribute in regions 1, 2, and 3, preventing over-exploration in any area.

Moreover, such policies could be quite different from a behavior standpoint and generate varied action sequences to visit unseen state-action pairs following the principle of optimism in the face of uncertainty [11, 8, 43].

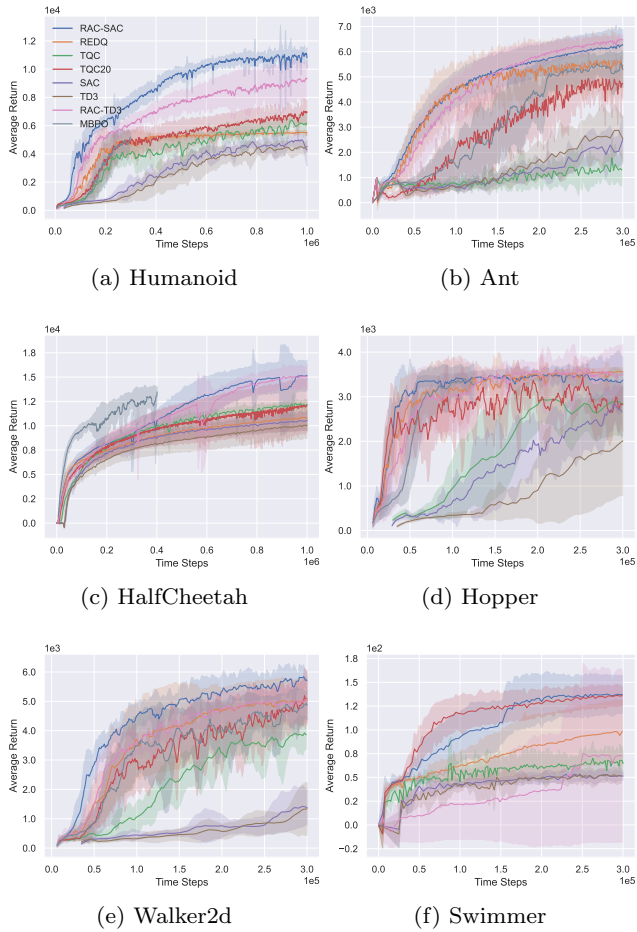


**Fig. 5** The learning curves on six Mujoco environments. The horizontal axis indicates the number of time steps. The vertical axis shows the average undiscounted return. The shaded areas denote one standard deviation over eight runs.

## 6 Experiments

We designed our experiments to answer the following questions:

- Can Realistic Actor-Critic outperform state-of-the-art algorithms in continuous control tasks?
- Can Realistic Actor-Critic better balance between value overestimation and underestimation?
- What is the contribution of each technique in Realistic Actor-Critic?

### 6.1 Setups

We implement RAC with SAC and TD3 as RAC-SAC(—) and RAC-TD3(—) (see Appendix B).

The baseline algorithms are REDQ [9](—), MBPO [22](—), SAC [19](—), TD3 [6](—) and TQC [10](—). All hyper-parameters we used for evaluation are the same as those in the original papers. For MBPO<sup>1</sup>, REDQ<sup>2</sup>, TD3<sup>3</sup> and TQC<sup>4</sup>, we use the authors' code. For SAC, we implement it following [19], and the results we obtained are similar to previously reported results. TQC20(—) is a variant of TQC with UTD  $G = 20$  for a fair comparison.

We compare baselines on six challenging continuous control tasks (Walker2d, HalfCheetah, Hopper, Swimmer, Ant, and Humanoid) from MuJoCo environments [21] in the OpenAI gym benchmark [20].

The time steps for training instances on Walker2d, Hopper, and Ant are  $3 \times 10^5$ , and  $1 \times 10^6$  for Humanoid and HalfCheetah. All algorithms explore with a stochastic policy but use a deterministic policy for evaluation similar to those in SAC. We report the mean and standard deviation across eight seeds.

For all algorithms, We use a fully connected network with two hidden layers, and 256 units per layer, with Rectified Linear Unit in each layer [47], for both actor and critic. All the parameters are updated by the Adam optimizer [48] with a fixed learning rate. All algorithms adopt almost the same NN architecture and hyperparameter.

For all experiments, our learning curves show the total undiscounted return.

Using the Monte Carlo method, we estimate the mean and std of normalized Q-function bias [9] as main analysis indicators to analyze the value approximation quality (described in Appendix A). The average bias lets us know whether  $Q_\theta$  is overestimated or underestimated, while std measures whether  $Q_\theta$  is overfitting.

Sample efficiency (SE) [9, 46] is measured by the ratio of the number of samples collected when RAC and

<sup>1</sup> <https://github.com/JannerM/mbpo>

<sup>2</sup> <https://github.com/watchernyu/REDQ>

<sup>3</sup> <https://github.com/sfujim/TD3>

<sup>4</sup> [https://github.com/SamsungLabs/tqc\\_pytorch](https://github.com/SamsungLabs/tqc_pytorch)

**Table 1** Performance on OpenAI Gym. The maximum value for each task is bolded.  $\pm$  corresponds to a single standard deviation over eight runs. The best results are indicated in bold. Results of SAC, TD3, and TQC are obtained at  $6 \times 10^6$  timesteps for Humanoid and HalfCheetah,  $3 \times 10^6$  timesteps for other environments. Results of RAC, REDQ, and TQC20 are obtained at  $1 \times 10^6$  timesteps for Humanoid and HalfCheetah and  $3 \times 10^5$  timesteps for other environments. Results of MBPO are obtained at  $3 \times 10^5$  timesteps for Ant, Humanoid, and Walker2d,  $4 \times 10^5$  for HalfCheetah,  $1.25 \times 10^5$  for Hopper.

	RAC-SAC	RAC-TD3	REDQ	MBPO	TQC20	TD3	SAC	TQC
Humanoid	<b>11107<math>\pm</math>475</b>	9321 $\pm$ 1126	5504 $\pm$ 120	5162 $\pm$ 350	7053 $\pm$ 857	7014 $\pm$ 643	7681 $\pm$ 1118	10731 $\pm$ 1296
Ant	6283 $\pm$ 549	6470 $\pm$ 165	5475 $\pm$ 890	5281 $\pm$ 699	4722 $\pm$ 567	<b>6796<math>\pm</math>277</b>	6433 $\pm$ 332	6402 $\pm$ 1371
Walker	<b>5860<math>\pm</math>440</b>	5114 $\pm$ 489	5034 $\pm$ 711	4864 $\pm$ 488	5109 $\pm$ 696	4419 $\pm$ 1682	5249 $\pm$ 554	5821 $\pm$ 457
Hopper	3421 $\pm$ 483	3495 $\pm$ 672	<b>3563<math>\pm</math>94</b>	3280 $\pm$ 455	3208 $\pm$ 538	3433 $\pm$ 321	2815 $\pm$ 585	3011 $\pm$ 866
HalfCheetah	15717 $\pm$ 1063	15083 $\pm$ 1113	10802 $\pm$ 1179	13477 $\pm$ 443	12123 $\pm$ 2600	14462 $\pm$ 1982	16330 $\pm$ 323	<b>17245<math>\pm</math>293</b>
Swimmer	<b>143<math>\pm</math>6.8</b>	71 $\pm$ 83	98 $\pm$ 31	-	143 $\pm$ 9.6	53 $\pm$ 8.8	51 $\pm$ 4.2	65 $\pm$ 5.8

**Table 2** Sample efficiency comparison. Sample efficiency [9, 46] is measured by the ratio of the number of samples collected when RAC and some algorithms reach the specified performance. The last four rows show how many times RAC is more sample efficient than other algorithms in achieving that performance.

	RAC-SAC	REDQ	MBPO	TQC	TQC20	REDQ/RAC-SAC	MBPO/RAC-SAC	TQC/RAC-SAC	TQC20/RAC-SAC
Humanoid at 2000	63K	109K	154K	145K	147K	1.73	2.44	2.30	2.33
Humanoid at 5000	134K	250K	295K	445K	258K	1.87	2.20	3.32	1.93
Humanoid at 10000	552K	-	-	3260K	-	-	-	5.91	-
Ant at 1000	21K	28K	62K	185K	42K	1.33	2.95	8.81	2.00
Ant at 3000	56K	56K	152K	940K	79K	1.00	2.71	16.79	1.41
Ant at 6000	248K	-	-	3055K	-	-	-	12.31	-
Walker at 1000	27K	42K	54K	110K	50K	1.56	2.00	4.07	1.85
Walker at 3000	53K	79K	86K	270K	89K	1.49	1.62	10.75	1.68
Walker at 5000	147K	272K	-	960K	270K	1.85	-	6.53	1.84

some algorithm reach the specified performance. Hopper is not in the comparison object as the performance of algorithms is almost indistinguishable.

## 6.2 Comparative evaluation

**OpenAI Gym.** Figure 5 and Table 1 shows learning curves and performance comparison. RAC consistently improves the performance of SAC and TD3 across all environments and performs better than other algorithms. In particular, RAC learns significantly faster for Humanoid and has better asymptotic performance for Ant, Walker2d, and HalfCheetah. RAC yields a much smaller variance than SAC and TQC, indicating that the optimistic exploration helps the agents escape from bad local optima.

**Sample efficiency comparison.** Table 2 shows the sample efficiency comparison with baselines. Compared with TQC, RAC-SAC reaches 3000 and 6000 for Ant with 16.79x and 12.31x sample efficiency. RAC-SAC performs 1.5x better than REDQ halfway through training and 1.8x better at the end of training in Walker and Humanoid. They show that a better underestimation trade-off can achieve better sample-efficiency performance than the MuJoCo environments’ state-of-the-art algorithms.

**Value approximation analysis.** Figure 6 presents the results for Ant, Humanoid, and Walker2d.

In Ant and Walker2d, TQC20 has a high normalized mean of bias, indicating that TQC20 prevents catastrophic overestimation fails accumulation. TQC20 also has a high normalized std of bias, indicating that the bias is highly non-uniform, which can be detrimental. Since distributional RL is prone to overfitting with few samples, it may not be appropriate to use a high UTD ratio for TQC. In Humanoid, which has a high-dimensional state, overfitting still exists but has been alleviated.

Relative to TQC and TQC20, REDQ and RAC-SAC have a very low normalized std of bias for most of the training, indicating the bias across different state-action pairs is about the same. But the Q estimation of REDQ is too conservative in Humanoid, and the large negative bias makes REDQ trapped in a bad locally optimal policy, suffering from pessimistic underexploitation. For Ant and Walker2d, although this poor exploration does not harm the performance of the policy, it still slows down convergence speed compared to RAC.

Relative to REDQ, RAC-SAC keeps the Q bias nearly zero without overestimation accumulation; this benign overestimation bias significantly improves performance. RAC-SAC strikes a good balance between overestimation bias (good performance without being trapped in a bad local optima) and underestimation bias (slight overestimation bias and consistently small std of bias).

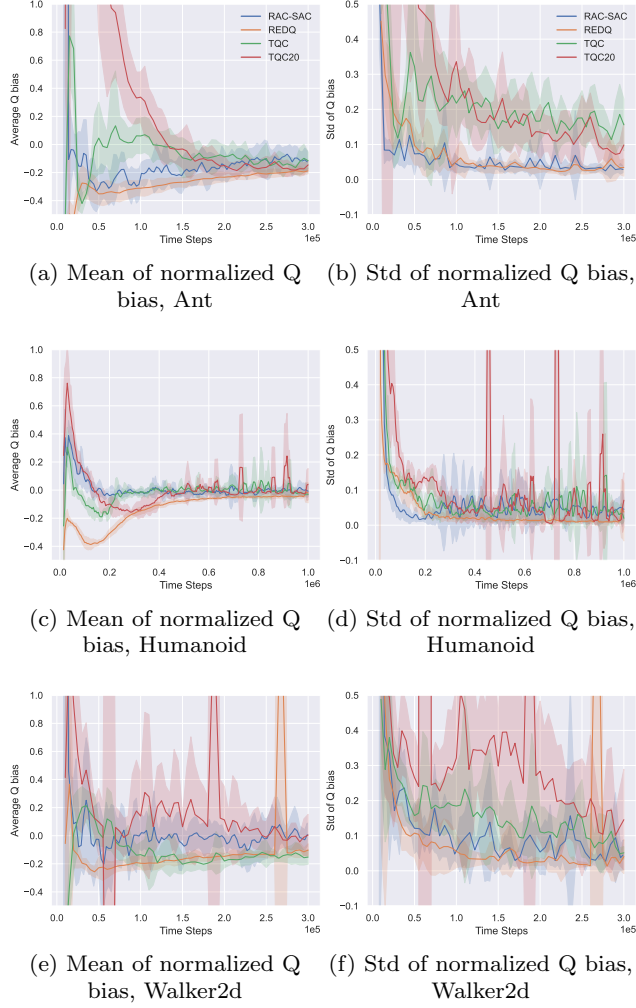


**Fig. 6** Estimated mean and std of normalized Q bias of RAC-SAC, REDQ, TQC, and TQC20 for Ant and Humanoid with Monte Carlo method.

### 6.3 Why Humanoid is hard for most baselines?

Figure 7 visualizes the performance respect to various value confidence bounds. Humanoid is extremely sensitive to value bias. The huge state-action space of Humanoid leads to a large approximation error of the value function with small samples. The approximate lower bound inevitably has the spurious maxima, while a small overestimated bias can seriously destabilize updates. It is hard to choose appropriate confidence bound for Humanoid by tuning the hyperparameters, resulting in a difficult under-overestimation trade-off.

Algorithms (like REDQ) that rely on constant hyperparameters to control the value bias have to conservatively introduce a large underestimation error (Figure 6) to stabilize updates, leading the policy to fall into pessimistic underexploration. In contrast, other al-

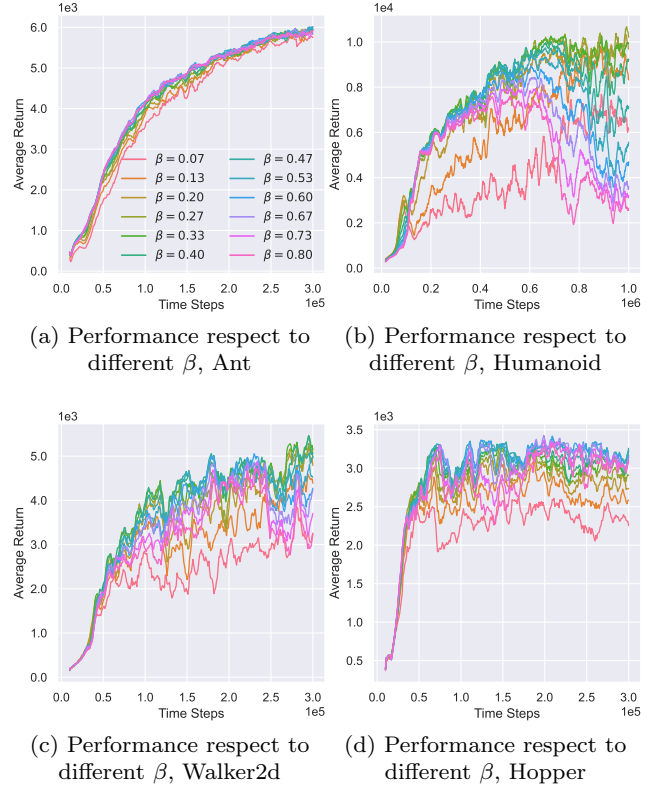


**Fig. 7** Performance of various value confidence bounds with respect to different  $\beta$ . We visualize different  $\beta$  belong to training distribution  $U_1 = \mathcal{U}[0, a]$  during training processes.

gorithms (such as TQC20) plagued by overestimation and overfitting require more samples.

Compared to Humanoid, the state-action space of other environments (see HalfCheetah and Swimmer in Appendix C) is much smaller. The approximate Q-functions can easily fit the true Q values accurately, significantly reducing the possibility of the spurious maxima. Therefore, optimistic exploration may not be a required component for these environments. So we can see that they are not very sensitive to various value confidence bound from figure 7. An underestimated value is enough to guide the policy to learn stably.

### 6.4 Variants of RAC

We evaluate the performance contributions of ingredients of RAC (—) (punished Bellman backup, policy family, optimistic exploration, independent temperature network, and learning rate warm-up) on a subset of four environments (see Figure 9).

**Punished Bellman backup (—).** When using the in-target minimization instead of punished Bellman backup, RAC is stable, but the performance is significantly worse

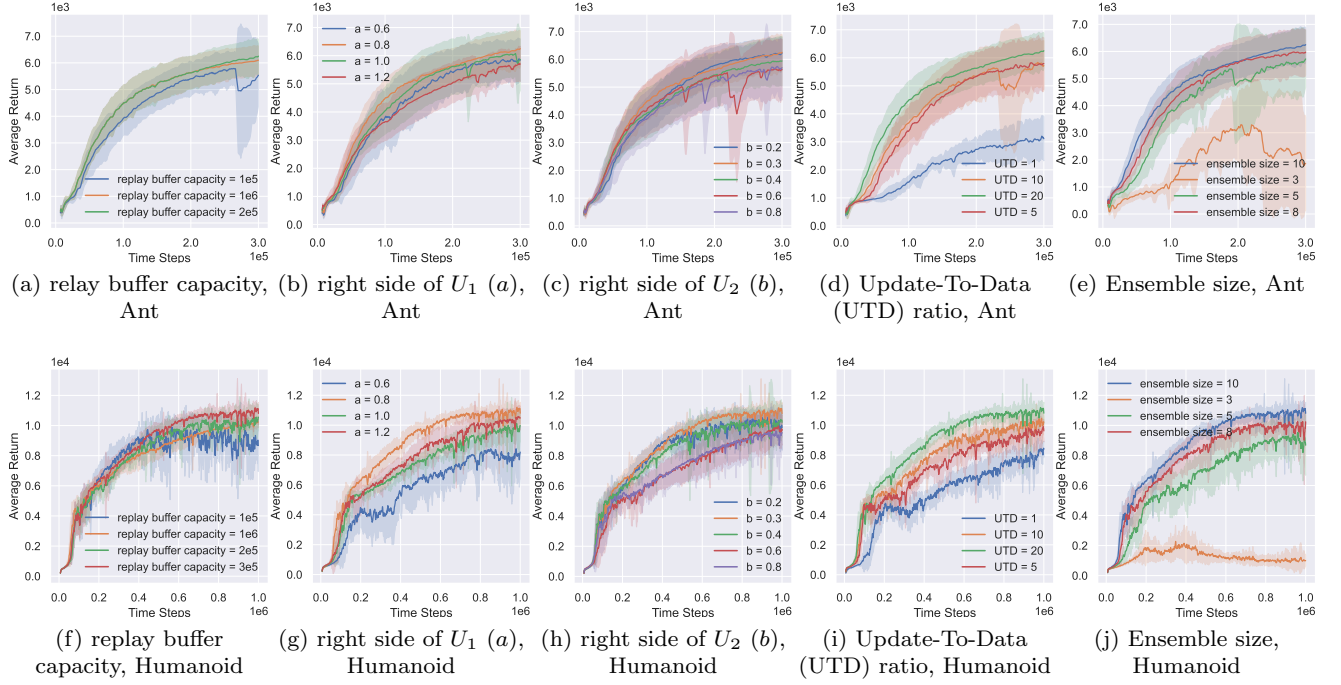


Fig. 8 Hyperparameter ablations of RAC.

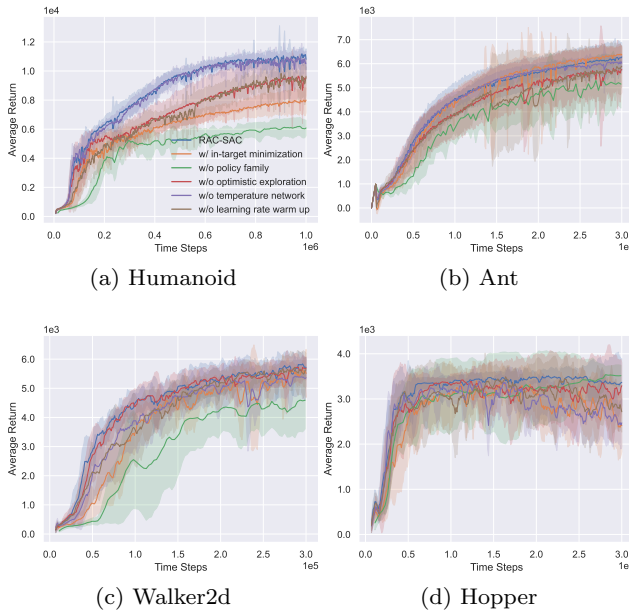


Fig. 9 Performance of RAC and its variants. The in-target minimization version of RAC is shown in Appendix B.4. RAC without policy family is named Vanilla RAC (details in Appendix B.3. In this case, OAC [11] is used as optimistic exploration method.)

in Humanoid. Punished Bellman backup provides more finer-grained bias control than in-target minimization, reducing the difficulty of learning representations. Compared with other environments, Humanoid has stronger

requirements for state representation learning [9]. Thus punished Bellman backup far outperforms in-target minimization in Humanoid and almost the same in other environments.

**Policy family (—).** The policy family is paramount to performance. This is consistent with Section 5.3’s conjecture. Even with OAC, agent can only converge to a local optimum without the policy family in Humanoid, indicating a single optimistic exploration method can not solve the pessimistic underexploration well. In addition, the convergence speed of the policy has decreased in Walker2d and Ant.

**Optimistic exploration (—).** Experimental results support the point in Section 6.3. Optimistic exploration can help the agent escape from local optima in Humanoid. But in simple environments (like Ant, Walker2d and Hopper), optimistic exploration has little impact on performance.

**Independent temperature network (—).** Except for Walker2d, the independent temperature network has little effect on RAC performance. The learned temperatures are shown in Appendix C. In practice, we find that the independent temperature network can control the entropy of the policy more quickly and stably.

**Learning rate warm-up (—).** A high UTD ratio can easily lead to an excessive accumulation of overestimation errors in the early stage of learning. The learning rate warm-up can alleviate this problem and

stabilize the learning process. Without the learning rate warm-up, RAC learns slower at the beginning of the training process.

### 6.5 Hyperparameter ablations

RAC introduces some hyperparameters, 1) replay buffer capacity, 2) right side of exploitation distribution  $U_1$  ( $a$ ), 3) right side of exploration distribution  $U_2$  ( $b$ ), 4) Update-To-Data (UTD) ratio  $G$  in Algorithm 1, 5) Ensemble size. Table 3 show that hyperparameters sweeps range, while Figure 8 show the numerical results.

**Table 3** Ablation study Hyperparameters Sweeps

Hyperparameters	Range
replay buffer capacity	$\{5 \times 10^4, 10^5, 2 \times 10^5, 3 \times 10^5, 10^6\}$
right side of $U_1$ ( $a$ )	$\{0.2, 0.3, 0.4, 0.6, 0.8\}$
right side of $U_2$ ( $b$ )	$\{0.4, 0.6, 0.8, 1.0, 1.2\}$
Update-To-Data (UTD) ratio $G$	$\{1, 5, 10, 20\}$
Ensemble size	$\{3, 5, 8, 10\}$

**Replay buffer capacity (Figure 8a and 8f).** RAC can benefit from a smaller capacity but will be hurt when the capacity is excessively small.

**right side of  $U_1$  ( $a$ ) (Figure 8b and 8g).**  $a$  is a key hyperparameter of RAC. Because  $a$  controls the underestimation bias of RAC, which determines the lower bound of Q-functions. The learning process becomes stable with  $a$  increasing. However, if  $a$  is too large, it will reduce the learning opportunity of optimistic policies, thereby reducing the learning efficiency.

**right side of  $U_2$  ( $b$ ) (Figure 8c and 8h).** Exploration policies become more conservative with  $b$  increasing, and the performance of RAC gradually declines. The increasing standard deviation means that more and more agents fall into local optimal policies. But if  $b$  is too small, policies may over-explore the overestimated state, resulting in a decrease in learning efficiency.

**The ensemble size (8e and 8j) and the UTD ratio (Figure 8d, 8i).** RAC appears to benefit greatly from The ensemble size and the UTD ratio. When the ensemble size and the UTD ratio are increased, we generally get a more stable average bias, a lower std of bias, and stronger performance.

## 7 Conclusions

This paper presents Realistic Actor-Critic(RAC) to improve the sample efficiency of existing off-policy actor-critic RL algorithms by effectively balancing value under- and overestimation. The proposed agent achieves high

scores and sample efficiency in four challenging mujoco benchmarks.

This work has three main contributions: (i) a framework for involving policies with different value confidence bonds. The exploratory nature of optimistic policies and the stability of pessimistic policies are considered. The method produces a way to auto-find the best value estimation degree in an unknown environment; (ii) a method for learning Q-functions, punished Bellman backup, provides fine-granular estimation bias control to make value approximation smoothly shift between upper bounds and lower bounds; (iii) Experiments show advantageous properties of RAC: low-value approximation error and brilliant sample efficiency. Furthermore, continuous control benchmarks suggest that RAC consistently improves performances and sample efficiency of existing off-policy RL algorithms, such as SAC and TD3.

Our results suggest that directly incorporating uncertainty to value functions and learning a powerful policy family can provide a promising avenue for improved sample efficiency and performance. Further exploration of ensemble methods, including high-level policies or more rich policy classes, is an exciting avenue for future work.

## 8 Conflict of interest

The authors declare that there is no conflict of interest.

## A Experiments Setups and methodology

### A.1 Evaluation method

For all training instances, the policies are evaluated every  $R_{eval} = 10^3$  time steps. The agent fixes its policy at each evaluation phase and deterministically interacts with the same environment, separate from obtaining 10 episodic rewards. The mean and standard deviation of these 10 episodic rewards is the performance metrics of the agent at the evaluation phase.

In the case of RAC, we employ a discrete number  $H$  of values  $\{\beta_i\}_{i=1}^H$  to get  $H$  policies:

$$\beta_i = b/H \cdot i, i = 1, \dots, H. \quad (17)$$

Each  $H$  policy fixes its policy at the evaluation phase and deterministically interacts with the environment with the fixed policy to obtain 10 episodic rewards. First, the 10 episodic rewards are averaged for each policy, and then the maximum of the 10-episode-average rewards of the  $H$  policies is taken as the performance at that evaluation phase.

We performed this operation for 8 different random seeds used in the computational packages(NumPy [49], PyTorch [50]) and environments(OpenAI gym [20]). The mean and standard deviation of the learning curve are obtained from these 8 simulations.

## A.2 The normalized value bias estimation

Given a state-action pair, the normalized value bias is defined as:

$$(\bar{Q}_\theta(\mathbf{s}, \mathbf{a}) - Q^\pi(\mathbf{s}, \mathbf{a})) / |E_{\bar{\mathbf{s}}, \bar{\mathbf{a}} \sim \pi} [Q^\pi(\bar{\mathbf{s}}, \bar{\mathbf{a}})]|, \quad (18)$$

where

- $Q^\pi(\mathbf{s}, \mathbf{a})$  be the action-value function for policy  $\pi$  using the standard infinite-horizon discounted Monte Carlo return definition.
- $\bar{Q}_\theta(\mathbf{s}, \mathbf{a})$  the estimated Q-value, defined as the mean of  $Q_{\theta_i}(\mathbf{s}, \mathbf{a}), i = 1, \dots, N$ .

For RAC, the normalized value bias is defined as:

$$(\bar{Q}_\theta(\mathbf{s}, \mathbf{a}, \beta^*) - Q^{\pi^*}(\mathbf{s}, \mathbf{a})) / |E_{\bar{\mathbf{s}}, \bar{\mathbf{a}} \sim \pi^*} [Q^{\pi^*}(\bar{\mathbf{s}}, \bar{\mathbf{a}})]|, \quad (19)$$

where

- $\pi^*$  is the best-performing policy in the evaluation among  $H$  policies A.1.
- $Q^{\pi^*}(\mathbf{s}, \mathbf{a})$  be the action-value function for policy  $\pi^*$  using the standard infinite-horizon discounted Monte Carlo return definition.
- $\bar{Q}_\theta(\mathbf{s}, \mathbf{a}, \beta^*)$  the estimated Q-value using  $Q_\theta$  of  $\beta^*$  which corresponds to the policy  $\pi^*$ , defined as the mean of  $Q_{\theta_i}(\mathbf{s}, \mathbf{a}, \beta^*), i = 1, \dots, N$ .

To get various target state-action pairs, we first execute the policy in the environment to obtain 100 state-action pairs and then sample the target state-action pair without repetition. Starting from the target state-action pair, run the Monte Carlo processes until the max step limit is reached. Table 4 lists common parameters of the normalized value bias estimation.

**Table 4** Parameters of the normalized value bias estimation

Parameter	Value
number of Monte Carlo process	20
number of target state-action pairs	20
Max step limit	1500

## B Hyperparameters and implementation details

We implement all RAC algorithms with Pytorch [50] and use Ray[tune] [51] to build and run distributed applications. For all the algorithms and variants, we first obtain 5000 data points by randomly sampling actions from the action space without making any parameter updates. Then, to stabilize the early learning of critics, a linear learning rate warm-up strategy is applied to critics in the start stage of training for RAC and its variants:

$$l = l_{init}(1 - p) + p \cdot l_{target}, p = \text{clip}\left(\frac{t - t_{start}}{t_{target} - t_{start}}, 0, 1\right), \quad (20)$$

where  $l$  is current learning rate,  $l_{init}$  is the initial value of learning rate,  $l_{target}$  is the target value of learning rate,  $t_{start}$  is the time steps to start adjusting the learning rate,  $t_{target}$  is the time steps to arrive at  $l_{target}$ .

For all RAC algorithms and variants, We parameterize both the actor and critics with feed-forward neural networks with 256 and 256 hidden nodes, respectively, with rectified linear units (ReLU) [52] between each layer.  $\beta$  is log-scaled before input into actors and critics. In order to prevent  $\beta$  sample from being zero, a small value  $\varepsilon = 10^{-7}$  is added to the left side of  $U_1$  and  $U_2$  to be  $U_1[\varepsilon, a]$  and  $U_2[\varepsilon, b]$ . Weights of all networks are initialized with Kaiming Uniform Initialization [53], and biases are zero-initialized. We normalize actions to a range of  $[-1, 1]$  for all environments.

### B.1 RAC-SAC algorithm

Here, the policy is modeled as a Gaussian with mean and covariance given by neural networks to handle continuous action spaces. The way RAC optimizes the policy makes use of the reparameterization trick [54, 19], in which a sample is drawn by computing a deterministic function of the state, policy parameters, and independent noise:

$$\tilde{\mathbf{a}}_\phi(\mathbf{s}, \beta, \xi) = \tanh(\mu_\phi(\mathbf{s}, \beta) + \sigma_\phi(\mathbf{s}, \beta) \odot \xi), \quad \xi \sim \mathcal{N}(0, I). \quad (21)$$

The actor network outputs the Gaussian's means and log-scaled covariance, and the log-scaled covariance is clipped in a range of  $[-10, 2]$  to avoid extreme values. Then, the actions are bounded to a finite interval by applying an invertible squashing function ( $\tanh$ ) to the Gaussian samples, and the Squashed Gaussian Trick [19] calculates the log-likelihood of actions.

**Algorithm 2** RAC: TD3 version

---

```

1: Initialize actor network  $\phi$ 
2: Initialize  $N$  critic networks  $\theta_i, i = 1, \dots, N$ 
3: Initialize empty replay buffer  $\mathcal{B}$ 
4: Initialize target network  $\bar{\theta}_i \leftarrow \theta_i$ , for  $i = 1, 2, \dots, N$ 
5: Initialize uniform distribution  $U_1$  and  $U_2$ 
6: for each iteration do
7:   execute an action:
8:    $\mathbf{a} = \pi_\phi(\cdot | \mathbf{s}, \beta) + \epsilon, \epsilon \sim \mathcal{N}(0, \sigma), \beta \sim U_2$ .
9:   Observe reward  $r$ , new state  $\mathbf{s}'$ 
10:  Store transition tuple  $\mathcal{B} \leftarrow \mathcal{B} \cup \{(\mathbf{s}, \mathbf{a}, r, \mathbf{s}')\}$ 
11:  for  $G$  updates do
12:    Sample random minibatch:
13:     $\{\tau_j\}_{j=1}^B \sim \mathcal{B}, \{\beta_m\}_{m=1}^B \sim U_1$ 
14:    Compute the Q target (23)
15:    for  $i = 1, \dots, N$  do
16:      Update  $\theta_i$  by minimize  $\mathcal{L}_{\text{critic}}^{\text{RAC}}$  (14)
17:      Update target networks:
18:       $\bar{\theta}_i \leftarrow \rho \bar{\theta}_i + (1 - \rho) \theta_i$ 
19:    Update  $\phi$  by minimize  $\mathcal{L}_{\text{actor}}^{\text{RAC-TD3}}$  (26)

```

---

The temperature is parameterized by a one-layer feedforward neural network  $T_\psi$  of 64 with rectified linear units (ReLU). To prevent temperature be negative, we parameterize temperature as:

$$\alpha_\psi(\beta) = e^{T_\psi(\log(\beta)) + \xi}, \quad (22)$$

where  $\xi$  is constant controlling the initial temperature,  $\log(\beta)$  is log-scaled  $\beta$ ,  $T_\psi(\log(\beta))$  is the output of the neural network.

**B.2 RAC-TD3 algorithm**

We implement RAC-TD3 referring to <https://github.com/sfujim/TD3>. A final  $tanh$  unit following the output of the actor. Unlike TD3, we did not use a target network for the actor and delayed policy updates. For each update of critics, a small amount of random noise is added to the policy and averaged over mini-batches:

$$y = r + \gamma [\bar{Q}_\theta(\mathbf{s}', \mathbf{a}', \beta) - \beta \hat{s}(Q_\theta(\mathbf{s}', \mathbf{a}', \beta))], \quad (23)$$

$$\mathbf{a}' = \text{clip}(\pi_\phi(\cdot | \mathbf{s}', \beta) + \epsilon, -1, 1), \quad (24)$$

$$\epsilon \sim \text{clip}(\mathcal{N}(0, \sigma), -c, c). \quad (25)$$

The extended policy  $\pi_\phi$  is updated by minimizing the following object:

$$\mathcal{L}_{\text{actor}}^{\text{RAC-TD3}}(\phi) = \mathbb{E}_{\mathbf{s} \sim \mathcal{B}, \beta \sim U_1} [-\bar{Q}_\theta(\mathbf{a}, \mathbf{s}, \beta)], \mathbf{a} = \pi_\phi(\cdot | \mathbf{s}, \beta). \quad (26)$$

The pseudocode for RAC-TD3 is shown in Algorithm 2.

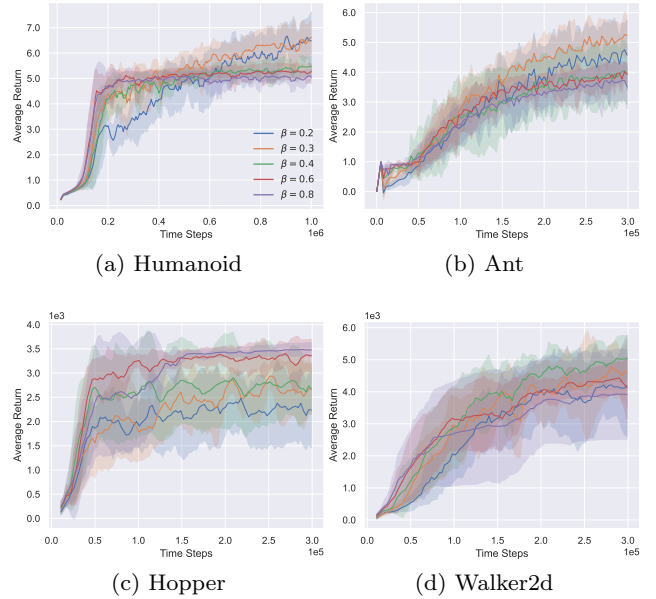


**Fig. 10** Performance of Vanilla RAC with different  $\beta$ .

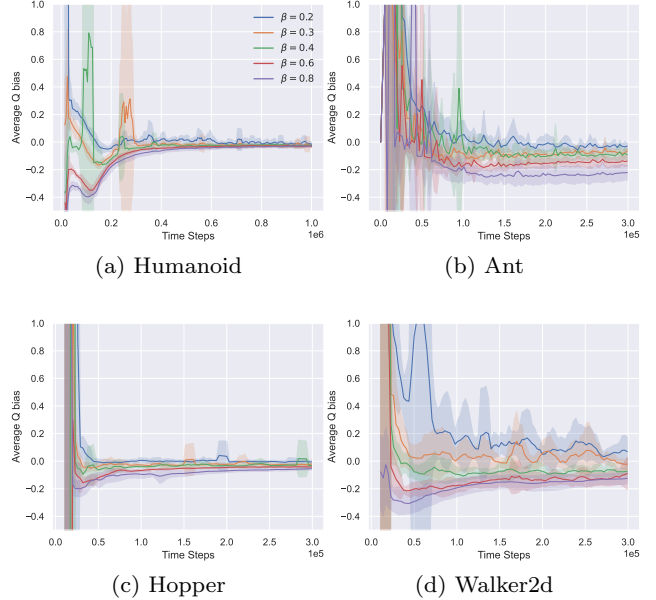


**Fig. 11** Mean of normalized Q bias for Vanilla RAC with different  $\beta$ .

**B.3 Vanilla RAC algorithm**

UVFA is not needed for vanilla RAC as  $\beta$  is a constant. The actor is updated by minimizing the following object:

$$\mathcal{L}_{\text{actor}}^{\text{vanillaRAC}}(\phi) = \mathbb{E}_{\mathbf{s} \sim \mathcal{B}, \mathbf{a} \sim \pi_\phi} [\alpha \log(\pi_\phi(\mathbf{a} | \mathbf{s})) - \bar{Q}_\theta(\mathbf{a}, \mathbf{s})]. \quad (27)$$

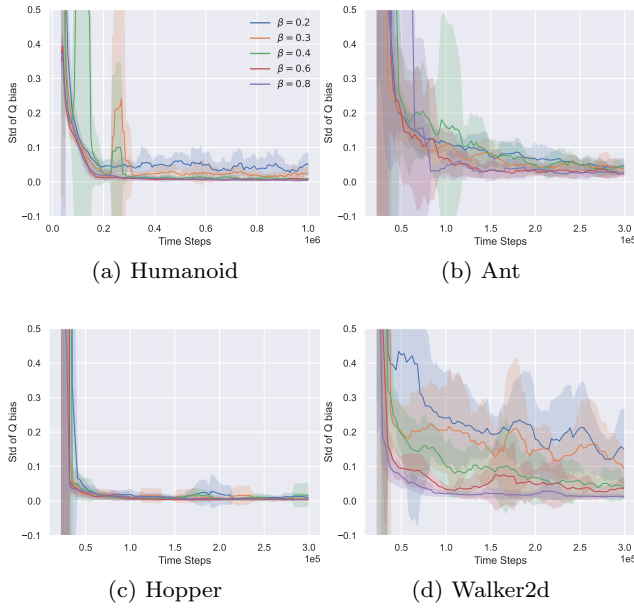


**Fig. 12** Std of normalized Q bias for Vanilla RAC with different  $\beta$ .

### Algorithm 3 Vanilla RAC

```

1: Initialize actor network  $\phi$ 
2: Initialize  $N$  critic networks  $\theta_i, i = 1, \dots, N$ 
3: Initialize empty replay buffer  $\mathcal{B}$ 
4: Initialize target network  $\bar{\theta}_i \leftarrow \theta_i$ , for  $i = 1, 2, \dots, N$ 
5: for each iteration do
6:   execute an action  $\mathbf{a} \sim \pi_\phi(\cdot | \mathbf{s})$ .
7:   Observe reward  $r$ , new state  $\mathbf{s}'$ 
8:   Store transition tuple  $\mathcal{B} \leftarrow \mathcal{B} \cup \{(\mathbf{s}, \mathbf{a}, r, \mathbf{s}')\}$ 
9:   for  $G$  updates do
10:    Sample random minibatch  $\{\tau_j\}_{j=1}^B \sim \mathcal{B}$ 
11:    Compute the Q target (7)
12:    for  $i = 1, \dots, N$  do
13:      Update  $\theta_i$  by minimize  $\mathcal{L}_{\text{critic}}$  (2)
14:      Update target networks:
15:       $\bar{\theta}_i \leftarrow \rho \bar{\theta}_i + (1 - \rho) \theta_i$ 
16:    Update  $\phi$  by minimize  $\mathcal{L}_{\text{actor}}^{\text{vanillaRAC}}$  (27)
17:    Update  $\alpha$  by minimize  $\mathcal{L}_{\text{temp}}$  (6)

```

The pseudocode for Vanilla RAC is shown in Algorithm 3. Figure 10, 11, and 12 shows performance and Q bias of Vanilla RAC with different  $\beta$ .

### B.4 RAC with in-target minimization

We implement RAC with in-target minimization referring to authors's code <https://github.com/watchernyu/REDQ>. The critics and actor are extended as  $Q_{\theta_i}(\mathbf{s}, \mathbf{a}, k)$  and  $\pi_\phi(\cdot | \mathbf{s}', k)$ ,  $U_1$  is a uniform training distribution  $\mathcal{U}[1, a]$ ,  $a > 1$ ,  $k \sim U_1$  that determine the size of the random subset  $\mathcal{M}$ . When  $k$  is not an integer, the size of  $\mathcal{M}$  will be sample beween  $\text{floor}(k)$  and  $\text{floor}(k+1)$  accord-

### Algorithm 4 RAC with in-target minimization

```

1: Initialize actor network  $\phi$ 
2: Initialize  $N$  critic networks  $\theta_i, i = 1, \dots, N$ 
3: Initialize temperature network  $\psi$ 
4: Initialize empty replay buffer  $\mathcal{B}$ 
5: Initialize target network  $\bar{\theta}_i \leftarrow \theta_i$ , for  $i = 1, 2, \dots, N$ 
6: Initialize uniform distribution  $U_1$  and  $U_2$ 
7: for each iteration do
8:   execute an action  $\mathbf{a} \sim \pi_\phi(\cdot | \mathbf{s}, k), k \sim U_2$ .
9:   Observe reward  $r$ , new state  $\mathbf{s}'$ 
10:  Store transition tuple  $\mathcal{B} \leftarrow \mathcal{B} \cup \{(\mathbf{s}, \mathbf{a}, r, \mathbf{s}')\}$ 
11:  for  $G$  updates do
12:    Sample random minibatch:
13:    // UPDATE CRITICS VIA IN-TARGET MINIMIZATION
14:     $\{\tau_j\}_{j=1}^B \sim \mathcal{B}, \{k_j\}_{j=1}^B \sim U_1$ 
15:    Sample a set  $\mathcal{M}$  of  $k$  distinct indices from  $\{1, 2, \dots, N\}$ 
16:    Compute the Q target (29)
17:    for  $i = 1, \dots, N$  do
18:      Update  $\theta_i$  by minimize  $\mathcal{L}_{\text{critic}}^{\text{RAC}}$  (30)
19:      Update target networks:
20:       $\bar{\theta}_i \leftarrow \rho \bar{\theta}_i + (1 - \rho) \theta_i$ 
21:    Update  $\phi$  by minimize  $\mathcal{L}_{\text{actor}}^{\text{RAC-SAC}}$  (31)
22:    Update  $\psi$  by minimize  $\mathcal{L}_{\text{temp}}^{\text{RAC}}$  (28)

```

ing to the Bernoulli distribution  $\mathcal{B}(p)$  with parameter  $p = k - \text{floor}(k)$ , where  $\text{floor}$  is a round-towards-zero operator.

An independent temperature network  $\alpha_\psi$  parameterized by  $\psi$  is updated with the following object:

$$\mathcal{L}_{\text{temp}}^{\text{RAC}}(\psi) = \mathbb{E}_{\mathbf{s} \sim \mathcal{B}, \mathbf{a} \sim \pi_\phi, k \sim U_1} [-\alpha_\psi(k) \log \pi_\phi(\mathbf{a} | \mathbf{s}, k) - \alpha_\psi(k) \mathcal{H}]. \quad (28)$$

In-target minimization is used to calculate the target  $y$ :

$$y = r + \gamma \mathbb{E}_{\mathbf{a}' \sim \pi_\phi} [\min_{i \in \mathcal{M}} Q_{\bar{\theta}_i}(\mathbf{s}', \mathbf{a}', k) - \alpha_\psi(k) \log \pi_\phi(\mathbf{a}' | \mathbf{s}', k)], \quad (29)$$

Then each  $Q_{\theta_i}(\mathbf{s}, \mathbf{a}, k)$  is updated with the same target:

$$\mathcal{L}_{\text{critic}}^{\text{RAC}}(\theta_i) = \mathbb{E}_{\tau_t \sim \mathcal{B}, k \sim U_1} [(Q_{\theta_i}(\mathbf{s}, \mathbf{a}, k) - y)^2]. \quad (30)$$

The extended policy  $\pi_\phi$  is updated by minimizing the following object:

$$\mathcal{L}_{\text{actor}}^{\text{RAC}}(\phi) = \mathbb{E}_{\mathbf{s} \sim \mathcal{B}, k \sim U_1} [\mathbb{E}_{\mathbf{a} \sim \pi_\phi} [\alpha_\psi(k) \log (\pi_\phi(\mathbf{a} | \mathbf{s}, k)) - \bar{Q}_\theta(\mathbf{a}, \mathbf{s}, k)]]]. \quad (31)$$

When interacting with the environment, obtaining exploration behaviors by sample  $k$  from exploration distribution  $U_2 = \mathcal{U}[1, b]$ ,  $a > b > 1$ .

The pseudocode for RAC with in-target minimization is shown in Algorithm 4.

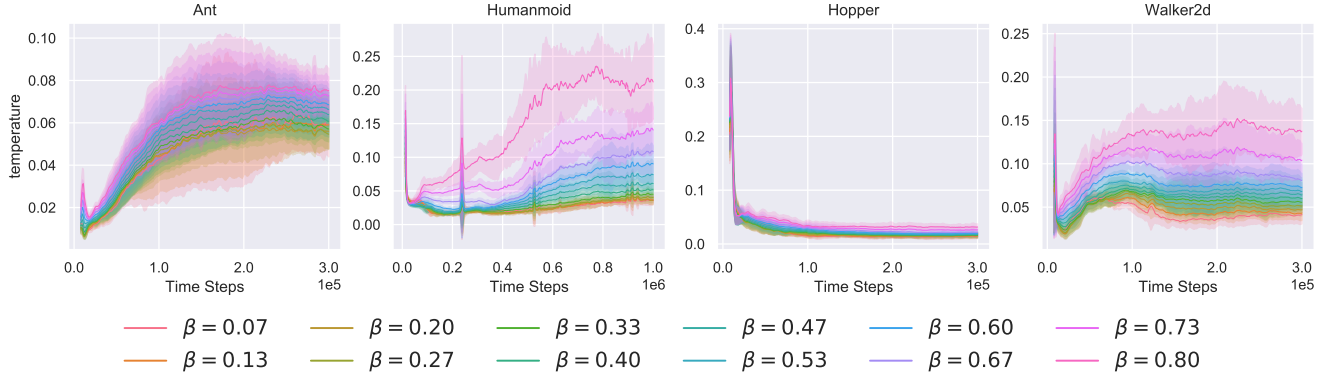


**Fig. 13** Visualisations of learned temperatures for RAC-SAC with different  $\beta$ .

**Table 5** Environment dependent hyperparameters

Hyperparameters	Humanoid	Walker	Ant	Hopper	HalfCheetah	Swimmer
<i>RAC-SAC</i>						
replay buffer capacity	$3 \times 10^5$	$10^5$	$2 \times 10^5$	$1 \times 10^6$	$2.5 \times 10^5$	$2 \times 10^5$
exploitation distribution $U_1$	$\mathcal{U}[10^{-7}, 0.8]$	$\mathcal{U}[10^{-7}, 0.8]$	$\mathcal{U}[10^{-7}, 0.8]$	$\mathcal{U}[10^{-7}, 0.8]$	$\mathcal{U}[10^{-7}, 0.3]$	$\mathcal{U}[10^{-7}, 0.8]$
exploration distribution $U_1$	$\mathcal{U}[10^{-7}, 0.3]$	$\mathcal{U}[10^{-7}, 0.3]$	$\mathcal{U}[10^{-7}, 0.3]$	$\mathcal{U}[10^{-7}, 0.3]$	$\mathcal{U}[10^{-7}, 0.1]$	$\mathcal{U}[10^{-7}, 0.3]$
<i>RAC-TD3</i>						
replay buffer capacity	$3 \times 10^5$	$10^5$	$2 \times 10^5$	$1 \times 10^6$	$2.5 \times 10^5$	$2 \times 10^5$
exploitation distribution $U_1$	$\mathcal{U}[10^{-7}, 0.8]$	$\mathcal{U}[10^{-7}, 0.8]$	$\mathcal{U}[10^{-7}, 0.8]$	$\mathcal{U}[10^{-7}, 0.8]$	$\mathcal{U}[10^{-7}, 0.3]$	$\mathcal{U}[10^{-7}, 0.8]$
exploration distribution $U_1$	$\mathcal{U}[10^{-7}, 0.3]$	$\mathcal{U}[10^{-7}, 0.3]$	$\mathcal{U}[10^{-7}, 0.3]$	$\mathcal{U}[10^{-7}, 0.3]$	$\mathcal{U}[10^{-7}, 0.1]$	$\mathcal{U}[10^{-7}, 0.3]$
<i>Vanilla RAC</i>						
replay buffer capacity	$10^6$	$10^6$	$10^6$	$10^6$	$10^6$	$10^6$
uncertainty punishment ( $\beta$ )	0.2	0.3	0.2	0.2	0.1	0.4
<i>RAC-in-target</i>						
replay buffer capacity	$3 \times 10^5$	$10^5$	$2 \times 10^5$	$1 \times 10^6$	$1 \times 10^6$	$1 \times 10^6$

**Table 6** Specific Hyperparameters

Hyperparameters	Value
<i>RAC-SAC</i>	
initial temperature coefficient ( $\xi$ )	-5
<i>RAC-TD3</i>	
exploration noisy	$\mathcal{N}(0, 0.1)$
policy noisy ( $\sigma$ )	0.2
policy noisy clip ( $c$ )	0.5
<i>Vanilla RAC</i>	
initial temperature	$\exp(-3)$
uncertainty punishment ( $\beta$ )	0.3
<i>RAC with in-target minimization</i>	
initial temperature coefficient ( $\xi$ )	-5
exploitation distribution $U_1$	$\mathcal{U}[1, 1.5]$
exploration distribution $U_2$	$\mathcal{U}[1, 2.0]$

**Table 7** Shared hyperparameters

Hyperparameters	Value
optimizer	Adam [48]
actor learning rate	$3 \times 10^{-4}$
temperature learning rate	$3 \times 10^{-4}$
initial critic learning rate ( $l_{init}$ )	$3 \times 10^{-5}$
target critic learning rate ( $l_{target}$ )	$3 \times 10^{-4}$
time steps to start learning rate adjusting ( $t_{start}$ )	5000
time steps to reach target learning rate ( $t_{target}$ )	$10^4$
number of hidden layers (for $\phi$ and $\theta_i$ )	2
number of hidden units per layer (for $\phi$ and $\theta_i$ )	256
number of hidden layers (for $T_\psi$ )	1
number of hidden units per layer (for $T_\psi$ )	64
discount ( $\gamma$ )	0.99
nonlinearity	ReLU
evaluation frequency	$10^3$
minibatch size	256
target smoothing coefficient ( $\rho$ )	0.005
Update-To-Data (UTD) ratio ( $G$ )	20
ensemble size ( $N$ )	10
number of evaluation episodes	10
initial random time steps	5000
frequency of delayed policy updates	1
log-scaled covariance clip range	$[-10, 2]$
number of discrete policies for evaluation ( $H$ )	12

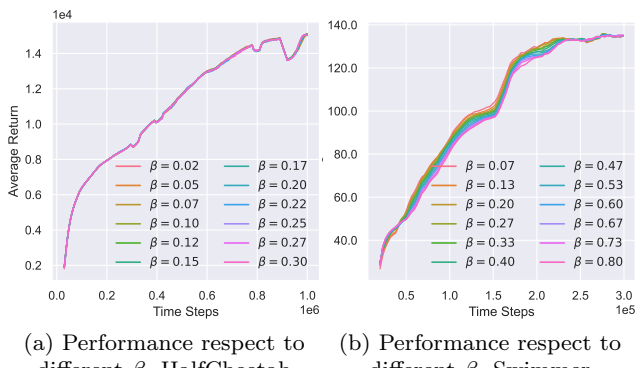


**Fig. 14** Performance of various value confidence bounds for different  $\beta$  for RAC-SAC. RAC leaners with a distribution of  $\beta$  instead of a constant  $\beta$ . We visualize different  $\beta$  belong to training distribution  $U_1 = \mathcal{U}[0, a]$  during training processes.

## B.5 Hyperparameter setting

Table 7 and 6 lists the hyperparameters for RAC and variants used in experiments.

## C Visualisations

**learned temperatures.** The Figure 13 shows the visualization of learned temperatures concerning different  $\beta$  during training. The figure demonstrates that learned temperatures are quite different. It is challenging to consider the temperature of different  $\beta$  with a single temperature.

### Performance of various value confidence bounds

The Figure 14 shows the performance of various value confidence bounds for different  $\beta$  for RAC-SAC on Half-Cheetah.

## Acknowledgment

The authors are grateful to the Editor-in-Chief, the Associate Editor, and anonymous reviewers for their valuable comments.

## References

- Levine S, Pastor P, Krizhevsky A, Ibarz J, Quillen D (2018) Learning hand-eye coordination for robotic grasping with deep learning and large-scale data collection. *The International journal of robotics research* 37(4-5):421–436
- Dulac-Arnold G, Levine N, Mankowitz DJ, Li J, Paduraru C, Gowal S, Hester T (2020) An empirical investigation of the challenges of real-world reinforcement learning. arXiv preprint arXiv:200311881
- Sutton RS, Barto AG (2018) Reinforcement learning: An introduction. MIT press
- Thrun S, Schwartz A (1993) Issues in using function approximation for reinforcement learning. In: Proceedings of the Fourth Connectionist Models Summer School, Hillsdale, NJ, pp 255–263
- Pendrith MD, Ryan MR, et al (1997) Estimator variance in reinforcement learning: Theoretical problems and practical solutions. University of New South Wales, School of Computer Science and Engineering
- Fujimoto S, Hoof H, Meger D (2018) Addressing function approximation error in actor-critic methods. In: International Conference on Machine Learning, PMLR, pp 1587–1596
- Lan Q, Pan Y, Fyshe A, White M (2020) Maxmin q-learning: Controlling the estimation bias of q-learning. arXiv preprint arXiv:200206487
- Lee K, Laskin M, Srinivas A, Abbeel P (2021) Sunrise: A simple unified framework for ensemble learning in deep reinforcement learning. In: International Conference on Machine Learning, PMLR, pp 6131–6141
- Chen X, Wang C, Zhou Z, Ross K (2021) Randomized ensembled double q-learning: Learning fast without a model. arXiv preprint arXiv:210105982
- Kuznetsov A, Shvechikov P, Grishin A, Vetrov D (2020) Controlling overestimation bias with truncated mixture of continuous distributional quantile critics. In: International Conference on Machine Learning, PMLR, pp 5556–5566
- Ciosek K, Vuong Q, Loftin R, Hofmann K (2019) Better exploration with optimistic actor critic. Advances in Neural Information Processing Systems 32
- Brafman RI, Tennenholtz M (2002) R-max-a general polynomial time algorithm for near-optimal reinforcement learning. *Journal of Machine Learning Research* 3(Oct):213–231
- Pathak D, Gandhi D, Gupta A (2019) Self-supervised exploration via disagreement. In: International Conference on Machine Learning, PMLR, pp 5062–5071
- Kim H, Kim J, Jeong Y, Levine S, Song HO (2019) Emi: Exploration with mutual information. In: International Conference on Machine Learning, PMLR, pp 3360–3369
- Schaul T, Horgan D, Gregor K, Silver D (2015) Universal value function approximators. In: International conference on machine learning, PMLR, pp 1312–1320

16. Badia AP, Sprechmann P, Vitvitskyi A, Guo D, Piot B, Kapturowski S, Tielemans O, Arjovsky M, Pritzel A, Bolt A, et al (2020) Never give up: Learning directed exploration strategies. arXiv preprint arXiv:200206038
17. Lyle C, Rowland M, Ostrovski G, Dabney W (2021) On the effect of auxiliary tasks on representation dynamics. In: International Conference on Artificial Intelligence and Statistics, PMLR, pp 1–9
18. Amos B, Dinh L, Cabi S, Rothörl T, Colmenarejo SG, Muldal A, Erez T, Tassa Y, de Freitas N, Denil M (2018) Learning awareness models. arXiv preprint arXiv:180406318
19. Haarnoja T, Zhou A, Hartikainen K, Tucker G, Ha S, Tan J, Kumar V, Zhu H, Gupta A, Abbeel P, et al (2018) Soft actor-critic algorithms and applications. arXiv preprint arXiv:181205905
20. Brockman G, Cheung V, Pettersson L, Schneider J, Schulman J, Tang J, Zaremba W (2016) Openai gym. arXiv preprint arXiv:160601540
21. Todorov E, Erez T, Tassa Y (2012) Mujoco: A physics engine for model-based control. In: 2012 IEEE/RSJ International Conference on Intelligent Robots and Systems, IEEE, pp 5026–5033
22. Janner M, Fu J, Zhang M, Levine S (2019) When to trust your model: Model-based policy optimization. Advances in Neural Information Processing Systems 32
23. Wu Y, Zhai S, Srivastava N, Susskind J, Zhang J, Salakhutdinov R, Goh H (2021) Uncertainty weighted actor-critic for offline reinforcement learning. arXiv preprint arXiv:210508140
24. Kumar A, Gupta A, Levine S (2020) Discor: Corrective feedback in reinforcement learning via distribution correction. Advances in Neural Information Processing Systems 33:18,560–18,572
25. Srivastava N, Hinton G, Krizhevsky A, Sutskever I, Salakhutdinov R (2014) Dropout: a simple way to prevent neural networks from overfitting. The journal of machine learning research 15(1):1929–1958
26. Wen Y, Tran D, Ba J (2020) Batchensemble: an alternative approach to efficient ensemble and lifelong learning. arXiv preprint arXiv:200206715
27. Abdar M, Pourpanah F, Hussain S, Rezazadegan D, Liu L, Ghavamzadeh M, Fieguth P, Cao X, Khosravi A, Acharya UR, et al (2021) A review of uncertainty quantification in deep learning: Techniques, applications and challenges. Information Fusion
28. Havasi M, Jenatton R, Fort S, Liu JZ, Snoek J, Lakshminarayanan B, Dai AM, Tran D (2020) Training independent subnetworks for robust prediction. arXiv preprint arXiv:201006610
29. Dusenberry M, Jerfel G, Wen Y, Ma Y, Snoek J, Heller K, Lakshminarayanan B, Tran D (2020) Efficient and scalable bayesian neural nets with rank-1 factors. In: International conference on machine learning, PMLR, pp 2782–2792
30. Wenzel F, Snoek J, Tran D, Jenatton R (2020) Hyperparameter ensembles for robustness and uncertainty quantification. Advances in Neural Information Processing Systems 33:6514–6527
31. Anschel O, Baram N, Shimkin N (2017) Averaged-dqn: Variance reduction and stabilization for deep reinforcement learning. In: International Conference on Machine Learning, PMLR, pp 176–185
32. Peer O, Tessler C, Merlis N, Meir R (2021) Ensemble bootstrapping for q-learning. arXiv preprint arXiv:210300445
33. Kalweit G, Boedecker J (2017) Uncertainty-driven imagination for continuous deep reinforcement learning. In: Conference on Robot Learning, PMLR, pp 195–206
34. Zheng12 Z, Yuan C, Lin12 Z, Cheng12 Y (2018) Self-adaptive double bootstrapped ddpg. International Joint Conference on Artificial Intelligence
35. Chen G, Peng Y (2019) Off-policy actor-critic in an ensemble: Achieving maximum general entropy and effective environment exploration in deep reinforcement learning. arXiv preprint arXiv:190205551
36. Badia AP, Piot B, Kapturowski S, Sprechmann P, Vitvitskyi A, Guo ZD, Blundell C (2020) Agent57: Outperforming the atari human benchmark. In: International Conference on Machine Learning, PMLR, pp 507–517
37. Saphal R, Ravindran B, Mudigere D, Avanchara S, Kaul B (2020) Seerl: Sample efficient ensemble reinforcement learning. arXiv preprint arXiv:200105209
38. Parker-Holder J, Pacchiano A, Choromanski KM, Roberts SJ (2020) Effective diversity in population based reinforcement learning. Advances in Neural Information Processing Systems 33:18,050–18,062
39. Jung W, Park G, Sung Y (2020) Population-guided parallel policy search for reinforcement learning. arXiv preprint arXiv:200102907
40. Osband I, Blundell C, Pritzel A, Van Roy B (2016) Deep exploration via bootstrapped dqn. Advances in neural information processing systems 29
41. Goyal A, Sodhani S, Binas J, Peng XB, Levine S, Bengio Y (2019) Reinforcement learning with competitive ensembles of information-constrained primitives. arXiv preprint arXiv:190610667
42. Rashid T, Peng B, Böhmer W, Whiteson S (2020) Optimistic exploration even with a pessimistic initialisation. In: International Conference on Learn-

ing Representations (ICLR)

- 43. Chen RY, Sidor S, Abbeel P, Schulman J (2017) Ucb exploration via q-ensembles. arXiv preprint arXiv:170601502
- 44. Ziebart BD (2010) Modeling purposeful adaptive behavior with the principle of maximum causal entropy. Carnegie Mellon University
- 45. Warwick DP, Lininger CA (1975) The sample survey: Theory and practice. McGraw-Hill
- 46. Dorner FE (2021) Measuring progress in deep reinforcement learning sample efficiency. arXiv preprint arXiv:210204881
- 47. Glorot X, Bordes A, Bengio Y (2011) Deep sparse rectifier neural networks. In: Proceedings of the fourteenth international conference on artificial intelligence and statistics, JMLR Workshop and Conference Proceedings, pp 315–323
- 48. Kingma DP, Ba J (2014) Adam: A method for stochastic optimization. arXiv preprint arXiv:14126980
- 49. Van Der Walt S, Colbert SC, Varoquaux G (2011) The numpy array: a structure for efficient numerical computation. Computing in science & engineering 13(2):22–30
- 50. Paszke A, Gross S, Massa F, Lerer A, Bradbury J, Chanan G, Killeen T, Lin Z, Gimelshein N, Antiga L, et al (2019) Pytorch: An imperative style, high-performance deep learning library. Advances in neural information processing systems 32
- 51. Liaw R, Liang E, Nishihara R, Moritz P, Gonzalez JE, Stoica I (2018) Tune: A research platform for distributed model selection and training. arXiv preprint arXiv:180705118
- 52. Nair V, Hinton GE (2010) Rectified linear units improve restricted boltzmann machines. In: Icml
- 53. He K, Zhang X, Ren S, Sun J (2015) Delving deep into rectifiers: Surpassing human-level performance on imagenet classification. In: Proceedings of the IEEE international conference on computer vision, pp 1026–1034
- 54. Kingma DP, Welling M (2013) Auto-encoding variational bayes. arXiv preprint arXiv:13126114